Nanoscale Res Lett (2009) 4:789–793
DOI 10.1007/s11671-009-9315-9

NANO EXPRESS

# Structural Modification in Carbon Nanotubes by Boron Incorporation

**Sangeeta Handuja · P. Srivastava · V. D. Vankar**

Received: 2 March 2009 / Accepted: 2 April 2009 / Published online: 25 April 2009


**Abstract** We have synthesized boron-incorporated carbon nanotubes (CNTs) by decomposition of ferrocene and xylene in a thermal chemical vapor deposition set up using boric acid as the boron source. Scanning and transmission electron microscopy studies of the synthesized CNT samples showed that there was deterioration in crystallinity and improvement in alignment of the CNTs as the boron content in precursor solution increased from 0% to 15%. Raman analysis of these samples showed a shift of $\sim 7$ cm$^{-1}$ in wave number to higher side and broadening of the G band with increasing boron concentration along with an increase in intensity of the G band. Furthermore, there was an increase in the intensity of the D band along with a decrease in its wave number position with increase in boron content. We speculate that these structural modifications in the morphology and microstructure of CNTs might be due to the charge transfer from boron to the graphite matrix, resulting in shortening of the carbon–carbon bonds.

**Keywords** Carbon nanotubes · Boron · Scanning electron microscopy · Transmission electron microscopy · Raman spectroscopy · X-ray diffractometry

## Introduction

Carbon nanotubes (CNTs), an allotrope of carbon, show modifications in properties when impurities like boron, nitrogen, and lithium are deliberately introduced in their matrix [1–3]. Defects generated in CNTs due to introduction of these impurities could offer a possible route to tune their structural, physical, and electronic properties and thus have a significant bearing on a broad range of applications [1–4]. For example, it is anticipated that the width of the band gap of the CNTs changes with addition of nitrogen and boron, which could lead to tailoring of electronic properties of the material [5].

Carbon has four valence electrons and boron has three; thus, a boron atom substituted into graphite (also an allotrope of carbon) lattice would tend to draw electrons from neighboring carbon atoms. This results in reduction in the reactivity of carbon atoms with electronegative oxygen atoms, and thus the decrease in oxidation of graphite [6]. Introduction of boron or nitrogen atoms could replace carbon atoms in CNTs resulting in modification in the number of charge carriers, which would eventually affect the electron field emission properties [7].

Boron can be incorporated into CNTs by various routes such as annealing CNTs with boron powder in a graphite crucible at high temperatures [8–11]. Chemical vapor deposition (CVD) method has also been employed for incorporation of boron in CNTs by using diborane as a source material [7]. Considering the fact that high temperature annealing causes defects into CNTs and diborane being very toxic gas, we have used boric acid, which is easy to handle, as the boron source. Furthermore, we have studied the structural modification in CNTs by varying the amount of boric acid. We show that the incorporation of small amount of boron during growth induces dramatic changes in CNT morphology.

## Experimental Details

The thermal CVD set up used for synthesis of CNTs has been described elsewhere [12]. In brief, it consisted of two

S. Handuja · P. Srivastava (✉) · V. D. Vankar
Nanostech Laboratory, Department of Physics, Indian Institute of Technology Delhi, Hauz-Khas, New Delhi 110016, India
e-mail: pankajs@physics.iitd.ernet.in

main components, namely, a furnace and a spray system consisting of a sprayer and a liquid reservoir. The one-stage tubular muffle furnace was of diameter 25.4 mm and length 220 mm. Inside this muffle was a quartz-tube of inner diameter 14 mm. The sprayer consisted of two concentric tubes with a nozzle of diameter 0.5 mm. The inner tube of the sprayer carried the solution from the reservoir to the nozzle of the sprayer. The nozzle end of the sprayer was fixed inside the quartz tube of the furnace (reactor). Argon (99.99% pure) was used as a carrier gas which flowed through the outer tube of the sprayer. It also exerted a pressure on the solution to regulate the liquid flow directed through the nozzle.

In a typical procedure, varying amounts of boric acid (5%, 10%, and 15%) was added to a fixed concentration of ferrocene and xylene solution (0.02 g/mL). After this, the solution was heated at around 100 °C to completely dissolve the boric acid and finally filtered using wattman filter paper of 0.1 pore size. The reactor was preheated to 950 °C and purged with Ar gas in order to create inert atmosphere. Subsequently, the solution from the reservoir was released at a constant rate and was atomized with the help of Ar gas till the temperature reaches to 900 °C. The soot film deposited on the reactor wall was later collected, by manually scratching the film. The samples grown with varying amounts of boric acid in the solution were named as B0NT, B5NT, B10NT, and B15NT indicating 0%, 5%, 10%, and 15% boric acid concentration, respectively.

The morphology of the grown CNT samples was studied using a scanning electron microscope (SEM: Stereo scan 360) operated at 15 kV. The microstructure of the samples was analyzed by high resolution TEM (HRTEM: Technai G2) operated at 200 kV. Raman spectroscopy (Micro-Raman T64000 Jobin Yvon triple monochromator system) was carried out at an excitation wavelength of 514.5 nm. The samples were also analyzed using X-ray diffractometry (XRD: Phillips Expert Pro-PW 3040). Elemental studies were done using energy dispersive X-ray spectroscopy (EDAX: Rontec, Quantex-Qx-1). For TEM analysis, samples were scratched from the quartz tube and were refluxed and ultrasonicated in ethanol for 3–4 h for proper dispersion. A few drops of the suspension were then transferred on to a carbon coated copper grid for TEM.

## Results and Discussion

Figure 1 shows the scanning electron micrographs of the samples B0NT, B5NT, B10NT, and B15NT. In all the micrographs, we find that bundles of CNTs are formed. However, from Fig. 1b, it is clear that at low concentration of boric acid (sample B5NT), CNTs are not well aligned. As the concentration of boric acid is increased to 10% (sample B10NT, Fig. 1c), alignment of the CNT bundles improves. In sample B15NT (Fig. 1d), they are found to be well aligned. It is found that in all the samples, the length of CNT is divided into two parts (shown by black arrows in Fig. 1), whereas for pure sample (B0NT), the length is altogether uniform. For lower concentration (B5NT), the top surface of the bundles shows the Y junction shape (Fig. 2a), as the concentration increases (B10NT and B15NT), The CNTs have the upper part as the agglomerated cauliflower-like structure (Fig. 2b, c). The length of the bundles of CNTs for samples B0NT, B5NT, B10NT, and B15NT as estimated from the SEM images are 25, 100, 120, and 125 μm, respectively.

TEM images for B0NT, B5NT, B10NT, and B15NT samples are shown in Fig. 3. It is evident from these micrographs that as the amount of boron in source solution increases, the crystallinity of the CNTs decreases, and more and more defects are incorporated in the samples. Based on TEM images, the diameter of the pure and boron-incorporated CNTs samples are found to be in the range of 40–60, and 10–40 nm, respectively. This indicates that boron-doped CNTs have smaller diameter than pure ones. Figure 4a represents the EDS spectrum for sample B10NT recorded by the EDAX system attached to the TEM. The spectrum clearly shows the presence of boron in the samples along with carbon, iron, copper, and silicon. In this sample, copper has come from the sample support grid TEM studies. It has also been observed that the intensity of the peak corresponding to boron increases with an increase in boron concentration in solution.

In contrast to previous reports [13], we have found, by using SEM and TEM techniques, that the crystallinity of CNTs deteriorates with increasing boron concentration. It is suggested from these studies that at lower concentration of boron, the boron atoms preferentially remain at the tip of the growing nanotubes with the tube body found to be of pure carbon as reported by other groups also [2]. At higher boron concentration, the boron atom propagates along the axis of the CNT with an increase at the tip. Considering this fact, we can clearly explain the structural modifications in samples B5NT, B10NT, and B15NT as being due to the incorporation of boron. We anticipate that at low concentration of boron, i.e., at 5% (B5NT) changes are observed only at the tip of CNTs (Figs. 1b, 2a). With more boron incorporated in the samples (B10NT and B15NT), more and more defects occur along the axis of nanotubes and the crystallinity is reduced (see Figs. 2b, c, 3c, d). It is also suggested that the partial replacement of carbon by boron in the nanotubes structure reduces the local hexagonal symmetry resulting in defects in the nanotubes [14].

Figure 5 shows the (002) Bragg's peak corresponding to graphite of pure as well as boron-incorporated CNT samples using the grazing incidence X-ray diffractometry

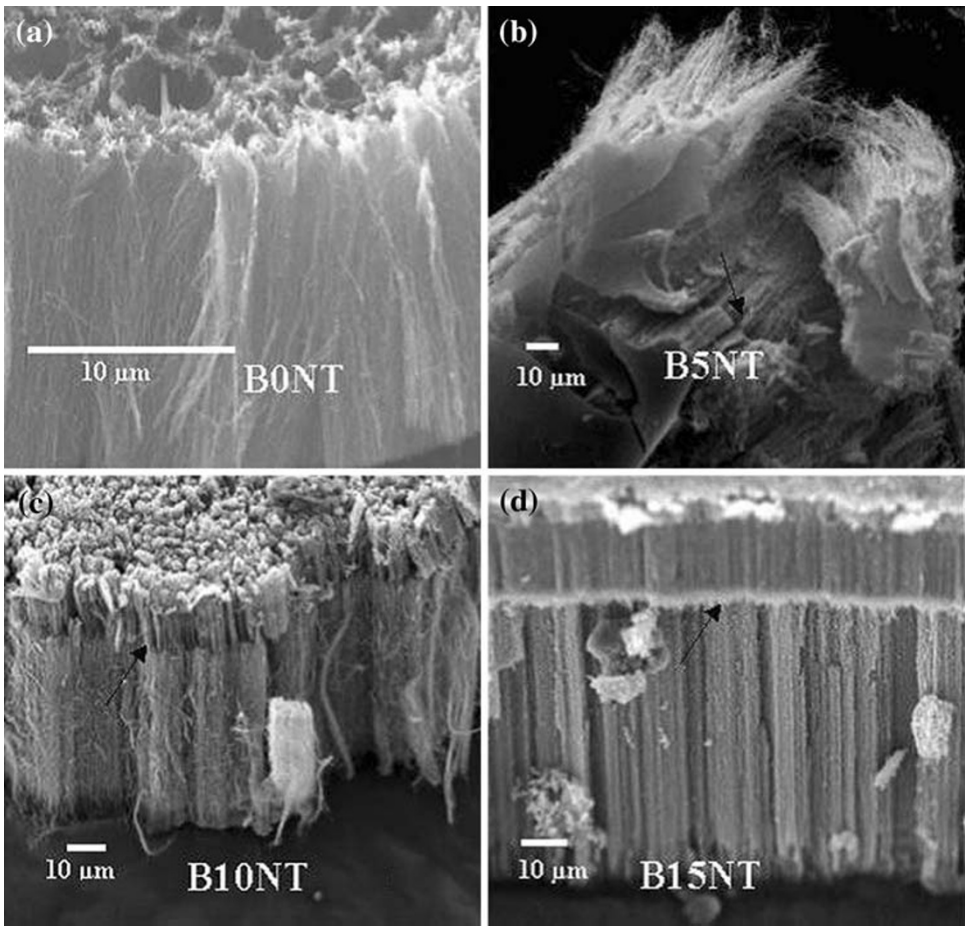


**Fig. 1** SEM images of pure and boron incorporated-MWNTs. **a** Without boron; **b**, **c,** and **d** 5%, 10%, and 15% boron in solution, respectively

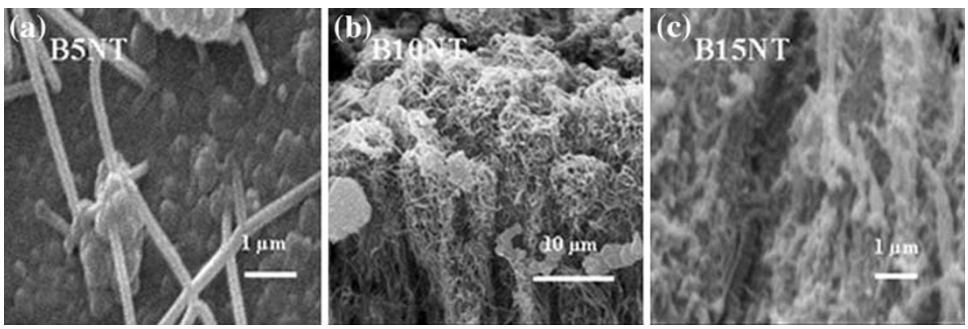


**Fig. 2** SEM images of upper surface of MWNTs with various amounts of boron

(GAXRD). This graphitic nature of the samples is mainly due to dissociation of carbon precursors at high temperature. It is inferred from the XRD results that Bragg's peak shifts to smaller scattering angle (larger plane spacing) and the full width at half maximum (FWHM) increases as the incorporation of boron in the CNTs increases [8, 15]. Increase in the "d" value (lattice spacing) for samples B5NT, B10NT, and B15NT as compared with sample B0NT could be attributed to the substitution of boron in the carbon.

Figure 6 shows Raman spectra for pure boron-incorporated CNT samples at 514.5-nm excitation wavelength. In the case of MWNTs, the Raman spectrum consists of two major peaks at $\sim$1,300 $cm^{-1}$, known as D band due to disorder and defects in MWNTs and at $\sim$1,570 $cm^{-1}$ and the G (graphitic) band due to lattice vibrations of the C–C bond. It is also evident from Fig. 7 that the intensity of the D band at $\sim$1,340 $cm^{-1}$ increases with an increase in boron concentration, whereas the intensity of G band hardly alters with increasing percentage of boron. Figure 7 shows an increase of the $I_D/I_G$ (intensity ratio of D and G bands) with increasing percentage of boron in the CNT samples, which is in accordance with earlier reports [16, 17]. Based on a Lorentzian line fit to the data (not shown

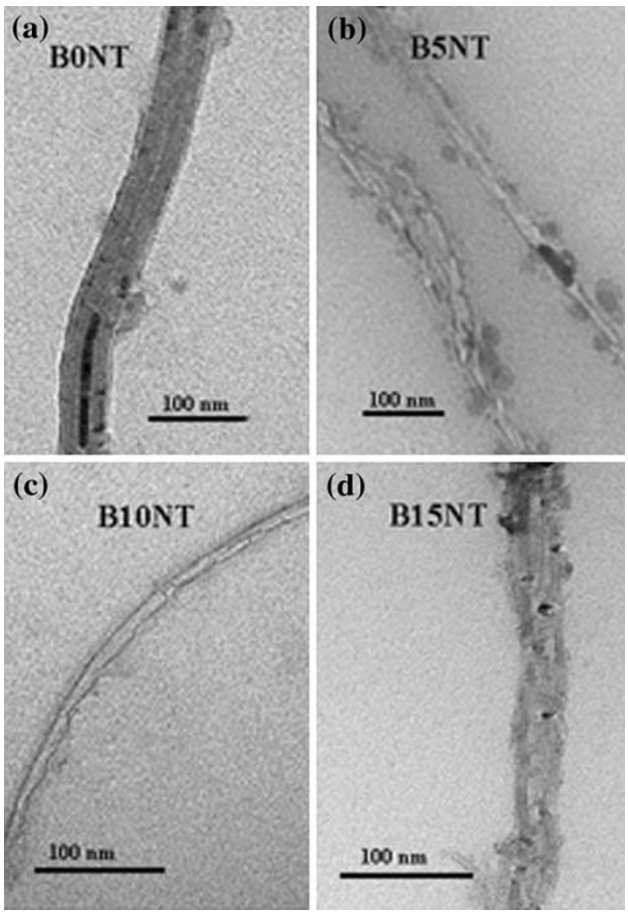


**Fig. 3** TEM images of pure and boron-incorporated MWNTs. **a** Without boron; **b**, **c,** and **d** 5%, 10%, and 15% boron in solution, respectively

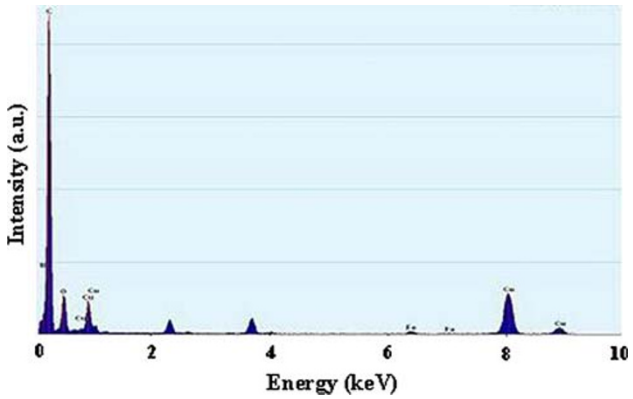


**Fig. 4** EDS spectra of sample B10NT

here), the G-band at $\sim$1,570 cm$^{-1}$ shows a significant shift (up to 7 cm$^{-1}$ from 0% to 15%) and broadening (increase in FWHM) with increase in the boron concentration. This is a clear indication that the nanotubes structure, as a whole, remains intact in CNT samples up to 15% boron in precursor, but at the same time defects in CNT samples

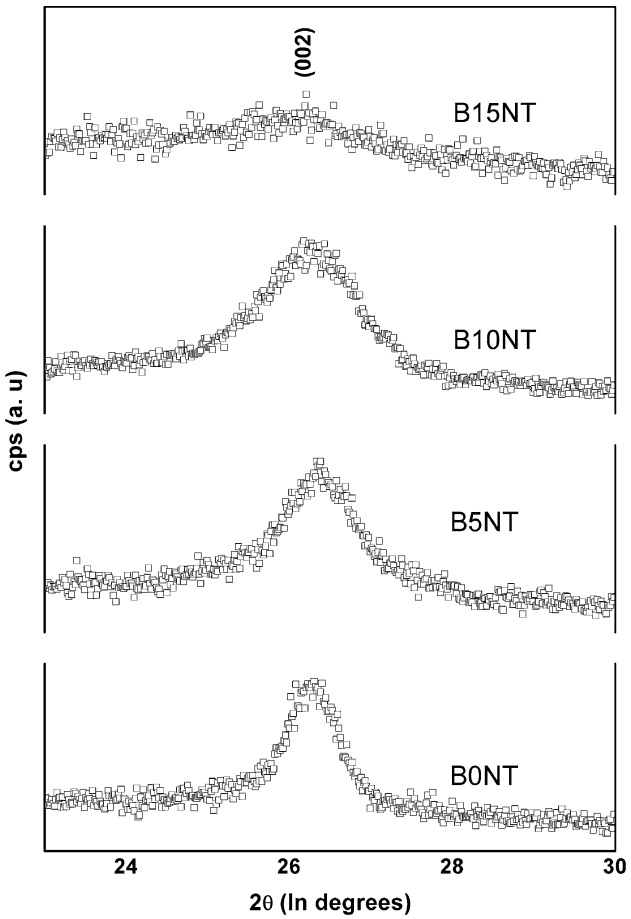


**Fig. 5** X-ray diffraction pattern for (002) plane of carbon for pure and boron-incorporated CNTs

increases as a function of boron concentration. This shift also indicates that charge carriers have been transferred from boron to the MWNTs, therby results in the shortening of the C–C bond which increases the force constant, and thus enhancing the lattice frequency of the MWNTs [16]. However, there is a decrease in D band position at $\sim$1,340 cm$^{-1}$ with increase in boron concentration, which is in agreement with reports given by Mondal et al. [18]. The shift in D band could be attributed to the presence of boron substitutions or the presence of defects such as vacancies.

## Conclusions

We have studied structural modifications in boron-incorporated CNTs. The EDS spectra of CNT samples were used to confirm the presence of boron. We found out that by increasing the boron concentration from 0% to 15% in the precursor solution, the alignment of the CNTs improves and the crystallinity of the samples deteriorates. At lower boron concentrations (at 5%), defects are only at the tip of

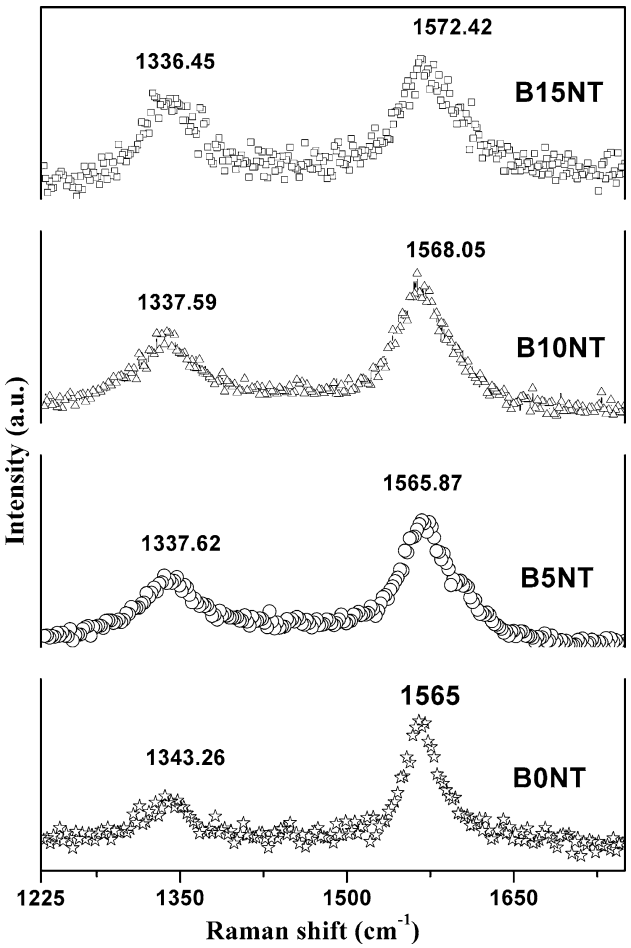


**Fig. 6** Raman spectra of CNTs with various concentrations of boron using 514.5-nm excitation wavelength

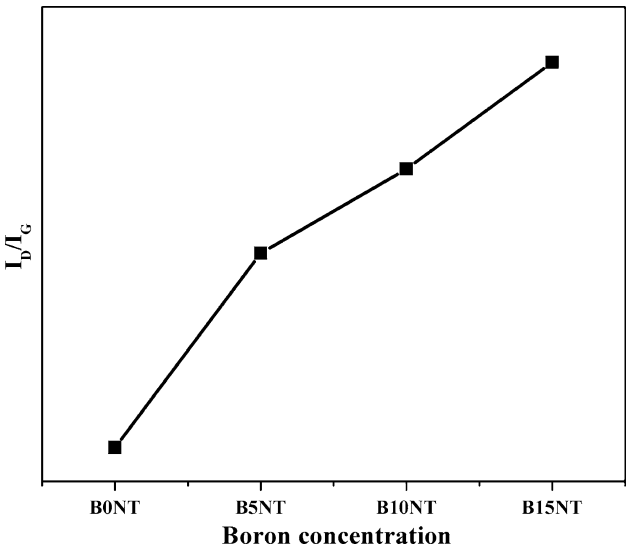


**Fig. 7** Variation of $I_D/I_G$ ratio with various boron concentrations

the CNTs. As the boron concentration increases, it is observed that the defects are also introduced along the axis of CNTs.

**Acknowledgment** One of the authors, Sangeeta Handuja is grateful to the Council of Scientific and Industrial Research (CSIR), Government of India for providing a research fellowship.

## References

1. M. Terrones, A.G.S. Filho, A.M. Rao, Book series Springer Berlin/Heidelberg. Top. Appl. Phys. **111**, 531 (2008). doi:10.1007/978-3-540-72865-8_17
2. W.K. Hsu, S. Firth, P. Redlich, M. Terrones, H. Terrones, Y.Q. Zhu, N. Grobert, A. Schilder, R.J.H. Clark, H.W. Krotoa, D.R.M. Waltona, J. Mater. Chem. **10**, 1425 (2000). doi:10.1039/b000720j
3. M. Baibarac, M.L. Cantú, J.O. Solé, N.C. Pastor, P.G. Romero, Small **2**, 1075 (2006). doi:10.1002/smll.200600148
4. L.H. Chan, K.H. Hong, D.Q. Xiao, W.J. Hsieh, S.H. Lai, H.C. Shiha, T.C. Lin, F.S. Shieu, K.J. Chen, H.C. Cheng, Appl. Phys. Lett. **82**, 4334 (2003). doi:10.1063/1.1579136
5. E.B. Palen, T. Pichler, A. Gra, R.J. Kalenczuk, M. Knupfer, J. Fink, Carbon **42**, 1123 (2004). doi:10.1016/j.carbon.2003.12.004
6. Q. Wang, L.Q. Chen, J.F. Annett, Phys. Rev. B **54**, R2271 (1996). doi:10.1103/PhysRevB.54.R2271
7. R.B. Sharma, D.J. Late, D.S. Joag, A. Govindaraj, C.N.R. Rao, Chem. Phys. Lett. **428**, 102 (2006). doi:10.1016/j.cplett.2006.06.089
8. W. Han, Y. Bando, K. Kurashima, T. Sato, Chem. Phys. Lett. **299**, 368 (1999). doi:10.1016/S0009-2614(98)01307-4
9. E. Borowiak-Palen, T. Pichler, G.G. Fuentes, A. Gra, R.J. Kalenczuk, M. Knupfer, J. Fink, Chem. Phys. Lett. **378**, 516 (2003). doi:10.1016/S0009-2614(03)01324-1
10. S. Ishii, T. Watanabe, S. Ueda, S. Tsuda, T. Yamaguchi, Y. Takano, Physica C **468**, 1210 (2008). doi:10.1016/j.physc.2008.05.034
11. D. Golberg, Y. Bando, K. Kurashima, T. Sato, Diam. Relat. Mater. **10**, 63 (2001). doi:10.1016/S0925-9635(00)00405-2
12. S. Handuja, P. Srivastava, V.D. Vankar, Synth. Reac. Inorg. Metal. Org. Nano Metal. Chem. **37**, 485 (2007). doi:10.1080/15533170701471786
13. P. Redlich, J. Loeffler, P.M. Ajayan, J. Bill, F. Aldinger, M. Riihle, Chem. Phys. Lett. **260**, 465 (1996). doi:10.1016/0009-2614(96)00817-2
14. D.L. Carroll, P. Redlich, X. Blase, J.C. Charlier, S. Curran, P.M. Ajayan, S. Roth, M. Rühle, Phys. Rev. Lett. **81**, 2332 (1998). doi:10.1103/PhysRevLett.81.2332
15. M. Sankaran, B. Viswanathan, Carbon **45**, 1628 (2007). doi:10.1016/j.carbon.2007.04.011
16. M.S. Dresselhaus, F.V. Paez, G.G. Samsonidze, S.G. Chou, G. Dresselhaus, J. Jiang, R. Saito, A.G.S. Filho, A. Jorio, M. Endo, Y.A. Kim, Physica E **37**, 81 (2007). doi:10.1016/j.physe.2006.07.048
17. J. Maultzsch, S. Reich, C. Thomsen, S. Webster, R. Czerw, D.L. Carroll, S.M.C. Vieira, P.R. Birkett, C.A. Rego, Appl. Phys. Lett. **81**, 2647 (2002). doi:10.1063/1.1512330
18. K.C. Mondal, A.M. Strydom, R.M. Erasmus, J.M. Keartland, N.J. Coville, Mater. Chem. Phys. **111**, 386 (2008). doi:10.1016/j.matchemphys.2008.04.034